Author/s:
Priscilla, N;Smith, D;Della Gaspera, E;Song, J;Wesemann, L;James, T;Roberts, A

Title:
Optical Janus Effect in Large Area Multilayer Plasmonic Films

Date:
2022

Citation:
Priscilla, N., Smith, D., Della Gaspera, E., Song, J., Wesemann, L., James, T. & Roberts, A. (2022). Optical Janus Effect in Large Area Multilayer Plasmonic Films. Advanced Photonics Research, 3 (5), pp.2100333-2100333. https://doi.org/10.1002/adpr.202100333.

Persistent Link:
https://hdl.handle.net/11343/299417

ADVANCED PHOTONICS RESEARCH
www.adpr-journal.com

Optical Janus Effect in Large Area Multilayer Plasmonic Films

*Niken Priscilla, Dan Smith, Enrico Della Gaspera, Jingchao Song, Lukas Wesemann, Timothy James, and Ann Roberts**

Plasmonic and other nanoparticles have attracted considerable interest for their role in structural coloration. The optical "Janus" effect, where the color of light reflected from a partially transmitting film depends on whether the device is viewed from the substrate or the coating side, is observed using a variety of nanostructured films. Herein, the optical Janus effect produced by homogeneous thin-film structures comprising only four layers of three different materials with a total thickness less than 300 nm is demonstrated. An asymmetric Fabry–Perot (FP) nanocavity is formed with a dielectric film bounded by two different metal films of nanoscale thickness. The semitransparent device has a transmitted color that is independent of the viewing direction. A broad color palette is available through the selection of various thicknesses and film materials. In addition to the directional optical effect, the device possesses iridescence properties and can generate images by selective removal of regions of one of the metallic films using simple photolithography. From a manufacturing perspective, this device is scalable and holds significant promise for applications in architecture, producing decorative features, and the development of overt and covert security features.

1. Introduction

Structural coloration, inspired by the biological world[1] is attracting increasing interest for its capacity to produce colored surfaces[2,3] and coatings.[4] Unlike potentially toxic pigments and dyes, they do not fade with time and can be produced with a reduced set of materials reducing costs associated with manufacturing. Typically, the structures of interest consist of either 1D or 2D gratings,[5,6] regular or random nanoparticle arrays,[7] or stacks of subwavelength thickness layers of materials with different refractive indices.[8] Interference and resonance effects lead to coloration. One particularly intriguing phenomenon has come to be known as the optical "Janus" effect (**Figure 1**), where the observed color of broadband light reflected from the device depends on whether it is illuminated from the substrate side or the other surface (referred to here as the "coating" side). Although reciprocity constraints ensure that the transmission through the device must be identical when illuminated from either side, the nonreciprocal relationship between the reflection from both sides is permitted through the presence of absorption.[9] The applications envisaged for these devices range from optical security features for documents and high-value goods,[10,11] windows tailored for thermal management of buildings,[12] and decorative coatings.[13,14]

To date, most demonstrations of this phenomenon have focused on the use of nanostructured films to create a layer with an effective refractive index. These have included the use of photonic crystals,[15] gold nanoparticles,[16] a textured Si_3N_4/Ag bilayer,[17] and single-crystal Cu_2O spheres.[18] England et al.[16] also examined the Janus effect in simple, non-patterned thin film stacks consisting of seven alternating layers of SiN and SiO_2 on a thin film of Cr supported by a glass substrate. Recent research has moved toward introducing a dynamic aspect to the phenomenon. Chen et al.[19] showed that a layer of WO_3 sandwiched between semitransparent indium tin oxide electrodes, and including a 3–4 nm thickness W layer on the substrate produced an

N. Priscilla, L. Wesemann, A. Roberts
ARC Centre of Excellence for Transformative Meta-Optical Systems
School of Physics
The University of Melbourne
Melbourne, Victoria 3010, Australia
E-mail: ann.roberts@unimelb.edu.au

The ORCID identification number(s) for the author(s) of this article can be found under https://doi.org/10.1002/adpr.202100333.

DOI: 10.1002/adpr.202100333

J. Song
School of Physics
The University of Melbourne
Melbourne, Victoria 3010, Australia

D. Smith
Melbourne Centre for Nanofabrication
151 Wellington Road, Clayton, Victoria 3168, Australia

E. Della Gaspera
School of Science
RMIT University
Melbourne, Victoria 3001, Australia

T. James
Reserve Bank of Australia
Craigieburn, Melbourne, Victoria 3064, Australia

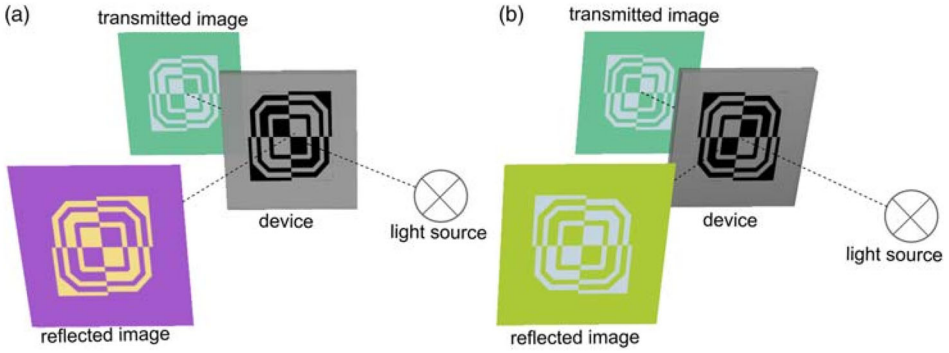

Figure 1. Visual demonstration of Janus effect where the reflected color depends on the viewing direction. Reflected and transmitted colors of the device as seen from: a) the "Coating" and b) the "substrate" sides of a semitransparent Janus device.

electrically tunable Janus effect. Porous Au-CYTOP-Au layers on a substrate were also shown to exhibit the Janus effect,[20] where the infiltration of liquids into the device changes the effective index of the dielectric layer with a corresponding change in the two reflected colors as well as the transmitted color. Since different structures generate colors with differing qualities, such as vibrancy and manufacturability,[21] exploring different approaches to generate the Janus effect is essential to improve the scalability and performance of the device.

In this work, the concept is extended to a simpler multilayer structure consisting of two thin layers of Ag and Cr and two layers of SiO_2 on a glass substrate which exhibits a striking color shift when viewed from either the substrate or the coating side (Figure 1). Vibrant reflection from both sides is achieved through the design of an asymmetric Fabry–Perot (FP) nanocavity formed by an insulator–metal–insulator–metal (I-MIM) structure. Numerical analysis and experimental studies are performed to investigate how the structure leads to a striking Janus effect. A selection of colors can be generated by tuning the geometry and materials that form the cavity. In addition, large area printing on the device is possible through selective removal of one of the metal films. The simple fabrication approach, with no requirement for high-resolution lithography techniques, is scalable. Hence, the device holds significant promise for use in decorative features for architectural and other applications and as optical security features.

2. Results and Discussion

The resonance wavelength of a metal–insulator–metal (MIM) structure is related to the accumulated phase associated with the optical thickness (the product of refractive index and physical thickness) of each layer and phase shifts associated with reflection from the various boundaries within the device. The saturation of the color, which is related to the spectral bandwidth can, in principle, be tailored by changing the thicknesses of the metallic layers. However, thickness variations also alter the accumulated phase and, thus, shift the resonance wavelength and change the color. To enhance the saturation of the device without moving the main resonance, phase compensation can be performed by integrating a dielectric capping layer (DCL) onto the MIM structure.[22] This layer also can be thought to act as an antireflection coating at the resonance, enhancing coupling to the cavity. The relationship between cavity resonance wavelength (λ_{res}) and the contributions to the accumulated phase of such a structure can be expressed as

$$\left(\frac{4\pi}{\lambda_{res}}\right) n_c t_c + \phi_a + \phi_r = 2m\pi \tag{1}$$

where m is an integer, n_c and t_c are the refractive index (at resonance) and thickness of the cavity spacing, respectively, and ϕ_a and ϕ_r represent phase shifts introduced by the strongly absorbing and higher reflecting layers that form the cavity boundaries. There will be phase and amplitude differences between the partial waves reflected from the first metallic film intercepted by an incident optical field when the device is illuminated from either the front or back. This influences the interference between this field and that reflected from the cavity producing an asymmetry in reflection at resonance, although the resonance condition is independent of the direction of incidence. This will result in different colors being reflected from the opposite sides. In addition to the improvement in saturation of the color when seen from the coating side, the DCL forms a protective layer preventing degradation of the silver film.[23] More details regarding the mechanism underpinning the Janus effect generated in this structure are provided in the Supporting Information.

The device considered (**Figure 2**a) consists of an SiO_2 capping layer of thickness t_{DCL}, with a cavity formed by a t_c thick film of SiO_2 bounded by an Ag layer (thickness t_r) and a Cr layer of thickness t_a. The structure is supported by a dielectric substrate taken here to have a refractive index of $n = 1.5$. The calculated reflectance from, absorption by, and transmission through a device with $t_{DCL} = 50\,nm$, $t_r = 20\,nm$, $t_c = 150\,nm$ and $t_a = 10\,nm$ from the film side (Figure 2b) and the substrate side (Figure 2c) are presented. The optical response of the device is mapped to a coordinate in the 1931 CIE diagram, assuming a standardized daylight broadband illumination spectra (D65), to predict its color. Simulations were performed using a rigorous, analytic transfer-matrix[24] approach and show that having a high index absorbing metal film is the key factor in producing a striking asymmetric color effect.

These calculations show that when light enters the FP cavity via the reflective layer (when illuminated from the coating side),

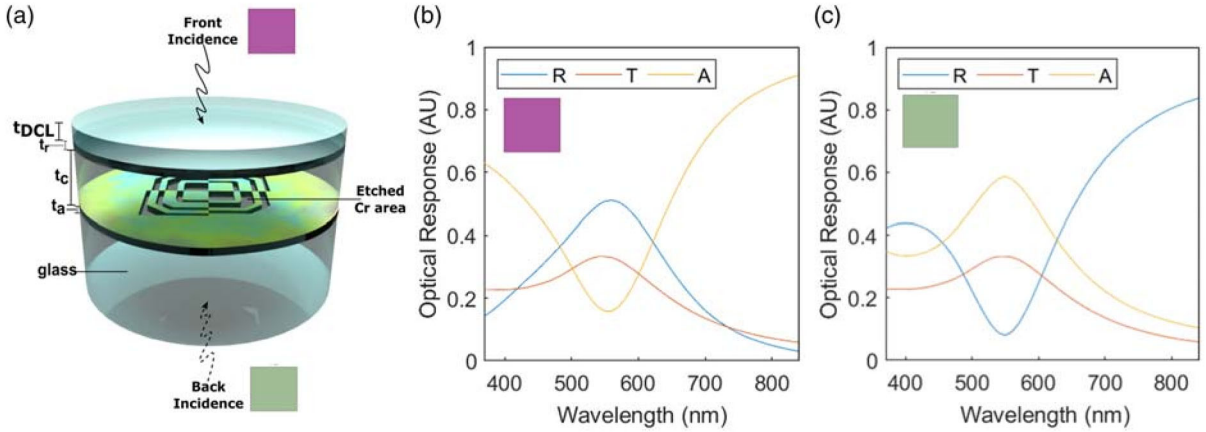

Figure 2. Design of the Janus device. Colors are calculated based on normal incidence. a) Schematic structure of the device. Reflectance (R), Transmittance (T), and Absorbance (A) spectra of the I-MIM films at normal incidence for: b) front incidence and c) back incidence.

wavelengths near the cavity resonance ($\lambda \approx 550$ nm) are selectively absorbed while the remainder of the spectrum is reflected or transmitted. The reflectance spectrum exhibits a minimum at this resonance wavelength, which corresponds to a pale magenta as seen in the CIE diagram (Figure 2b). For incidence from the substrate side, light enters the cavity via the thin absorbing layer. The calculated optical response now exhibits an absorbance minimum and a reflectance maximum at the resonance wavelength near 550 nm with a slight broadening compared to the case of incidence from the coating side (Figure 2c). This produces a green color. The appearance of a reflectance maximum by an opaque MIM structure with a similar combination of materials consisting of absorbing metal–dielectric–reflective metal is also found in the work of Kim et al.,[25] although the Janus color effect was not the focus.

Different geometries and materials can be utilized to engineer the colors of the Janus I-MIM device. The effect of varying the complex refractive indices[26–30] of each component of the design on the device performance as well as materials realizing the values are presented in **Figure 3**. Figure 3a shows that there is no asymmetric color effect when the absorbing metal layer is replaced by non-absorbing dielectric materials such as SiO_2, SiN, or TiO_2. The Janus effect with a weak color difference seems to emerge for theoretical dielectric materials with a high real part of the refractive index ($n \geq 4$). Metals with a high real part of the refractive index such as chromium and germanium were shown to create a more striking color asymmetry. This result supports previous findings,[16] which stated that placing an absorbing material between the dielectric film and the substrate is the key to generating the optical Janus color effect. Furthermore, in the presence of an absorbing layer with a high real part of the refractive index (e.g., Cr), asymmetric effects still occur over a wide range of reflective metal layer refractive indices (Figure 3b). Nevertheless, materials with a low real part of the refractive index such as silver and aluminum are preferred to maintain the color brightness and semi-transparency of the device. There is some flexibility in the choice of the dielectric materials. Figure 3c demonstrates that dielectric films with refractive indices ranging from $1.5 - 2.5$ are suitable for producing a variety of colors. Silica, silicon nitride, and titania are examples of dielectrics with refractive indices in this range. Thus, the color of the device can be tailored by selecting combinations of different materials and thicknesses. Silica was chosen here to simplify fabrication.

As mentioned previously, having an absorbing layer between the dielectric film and substrate is the key to generating the optical Janus effect. Furthermore, the resulting colors seen from either direction are highly sensitive to both the thickness and optical properties of this layer. Hence, if regions of the layer are selectively removed through, for example, photolithography. The cavity resonance is disrupted and the Janus effect disappears and a macroscopic-sized pattern can be observed by the unaided eye (Figure 2a). This feature is useful for applications in optical security devices or as decorative features.

Several samples with varying layer thicknesses were fabricated using an electron beam evaporator and plasma-enhanced chemical vapor deposition—details in the Experimental Section. Nominal thickness and material data are given in **Table 1**. In all designs considered, the thickness and composition of the DCL (SiO_2) are maintained at 50 nm. Photographs of the fabricated samples taken under broadband room illumination are presented with normalized reflectance data in **Figure 4**a and transmission data in Figure 4b. The reflectance and transmission measurements are taken at the angle of incidence of 6° due to instrument constraints. These are compared with simulated and experimentally obtained reflectance data in Figure 4a. The color seen from opposite sides of the sample demonstrates clear differences while maintaining semi-transparency with transmission data and sample images shown in Figure 4b. Images introduced into the structure by selectively etching the Cr layer can be clearly observed in Figure 4c–e. The typical feature size is $\approx 600\,mm^2$ (Figure S3, Supporting Information). Comparison of the reflected colors generated from the simulated and fabricated samples are presented in Figure 4a where the label **Sim.** refers to the simulation and **Exp.** denotes the color calculated from the measured spectra.

Asymmetric color effects are present in all samples as expected. Overall, the hues of the resulting colors are in

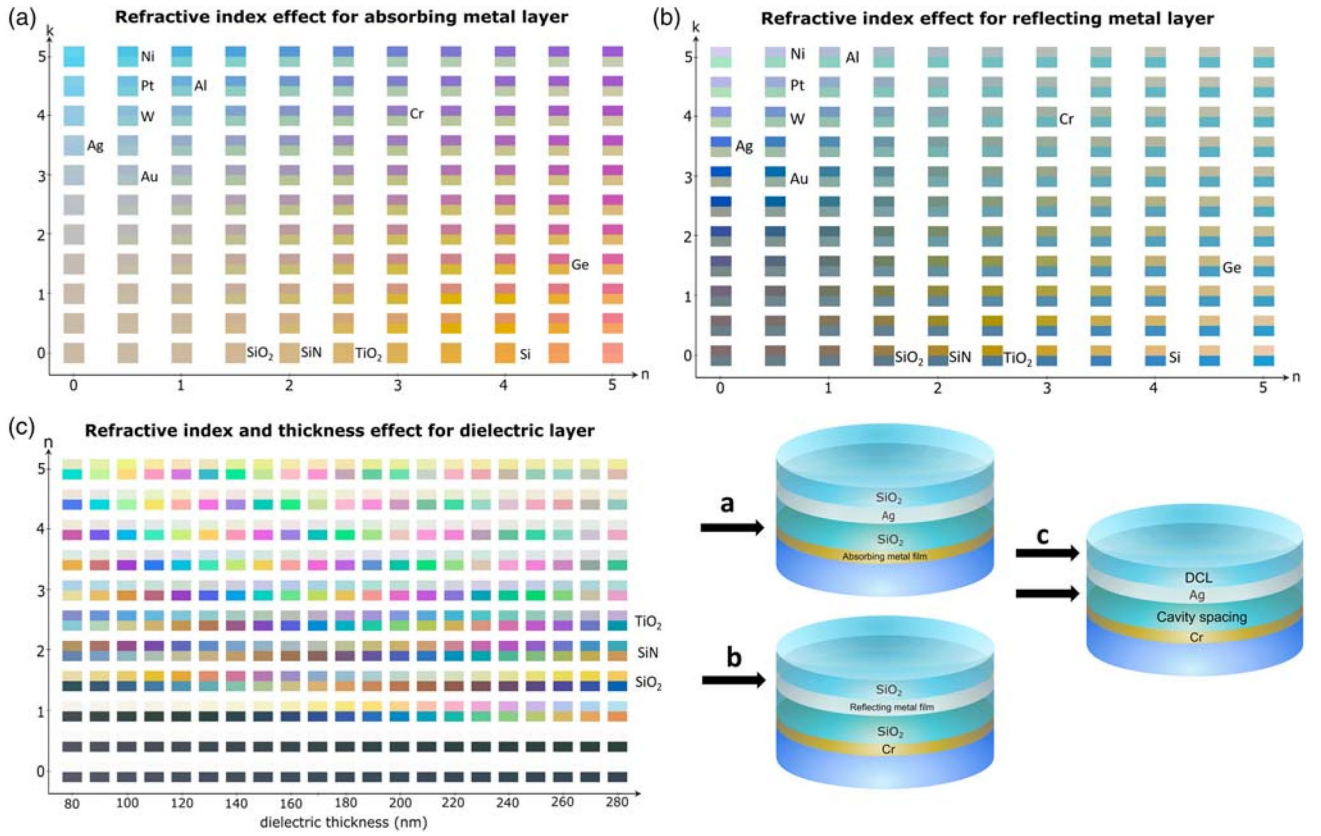

Figure 3. Refractive index effects on the: a) absorbing metal layer, b) reflecting metal layer, and c) cavity spacing of the Janus I-MIM device. Schematic diagrams on the bottom right show layers with varied refractive indexes. In a and b, the thicknesses of the *DCL* (t_{DCL}), reflective (t_r), silica (t_c), and absorbing (t_a) layers are kept constant at 50 nm–20 nm–150 nm–10 nm, respectively. Silver is used as the reflective layer for a, while chromium is used as the absorbing layer in b. The thickness of the insulating cavity layer is varied in c while keeping the other parameters constant. The *DCL* refractive index in this figure is adjusted to be the same as the cavity refractive index to permit comparison. For simplicity, the dispersive effect of the materials is omitted by taking the median values of n and k in the visible range (wavelengths of 370 – 840 nm).[26–30]

Table 1. Fabricated sample materials and thicknesses.

No.	Metal 1	Metal 2	t_a [nm]	t_r [nm]	t_c [nm]
1	Cr	Ag	10	20	110
2	Cr	Ag	10	20	130
3	Cr	Ag	10	20	150
4	Cr	Ag	10	20	180
5	Cr	Al	10	20	110
6	Cr	Al	10	20	130
7	Cr	Al	10	20	150
8	Cr	Ag	20	20	130
9	Cr	Al	20	10	130
10	Ag	Cr	20	10	110
11	Ag	Cr	20	10	150
12	Ag	Cr	20	10	180

reasonable agreement with simulations and the lithographically defined pattern is clearly apparent. In one group of samples, the thickness of the central SiO_2 layer is varied from 110 nm to 180 nm (Figure 4c). Increasing the cavity spacing results in different colors as shown. Due to the tolerances of the fabrication process, it was not possible to precisely replicate the design thickness of the silica layer. The thicknesses of the SiO_2 layers were measured following the chemical vapor deposition process (Table S1, Supporting Information) and used in the color calculation to compare the simulated and experimental results (Figure 4a). The general trends apparent in the measured reflectance spectra are consistent with those of the simulations, although discrepancies of up to 50 nm in features in the reflectance spectra along with spectral broadening of the experimentally obtained results (leading to a decrease in color saturation) can be seen. The simulation assumes perfectly homogeneous layers, but granulation can occur in fabricated thin films, particularly those with thicknesses below 30 nm.[25] This leads to variations in the effective refractive index of the materials, which are assumed to be those of bulk materials in simulations. Hue discrepancies are also observed between those recovered from the measured spectra (Figure 4a) and photographs (Figure 4c). Nevertheless, the striking Janus effect and the macroscopic patterns are clearly discernible to the unaided eye.

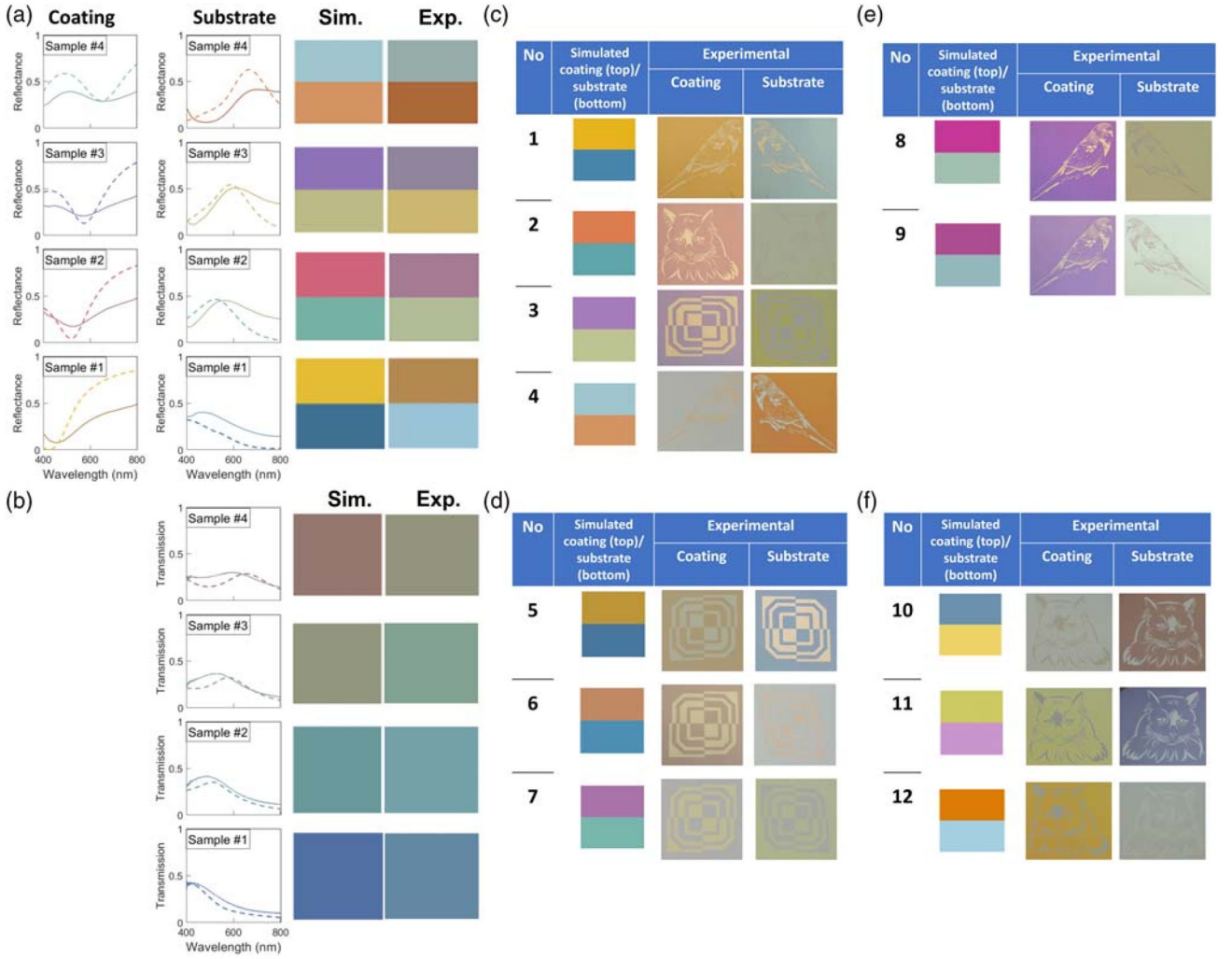

Figure 4. Measured (solid lines) and simulated (dashed lines): a) reflection and b) transmission spectra of samples 1 − 4 and the corresponding colors when illuminated from coating and substrate sides at near-normal incidence (6°). Ag and Cr films are used as the reflective and absorbing films, respectively, the silica cavity is varied in thickness. c) Color comparison between simulation (Sim.) and photographs (Exp.) of samples 1 − 4 under ambient light. Changes made to the structures: d) Al layer is used to replace Ag layer (samples 5–7), e) thickness of Cr layer is doubled (samples 8–9), f) the order of Cr and Ag layers are reversed (samples 10–12). Details about the device structure can be found in Table 1. The typical feature size used in all photographs is $\approx 600\,\text{mm}^2$ with a resolution of $5\,\mu\text{m}$ (Figure S3, Supporting Information).

Transmission measurement shows that the third color, independent of the viewing direction, is present in the devices. The trends seen in the transmission spectra are consistent with those predicted by the simulations (Figure 4b) and the experimentally obtained positions of the maxima are within $\pm 50\,\text{nm}$ of the predicted results. There is a slight decrease in the maximum transmitted intensity as the thickness of the cavity spacing increases over the range of values considered here, although all devices are transparent to some degree with peak transmittances varying between 30% and 40%.

Other samples were fabricated to investigate the replacement of 20 nm Ag with 10 nm Al (Figure 4d). This leads to a loss in saturation of the resulting color but the asymmetric color effect is retained. Increasing the thickness of the Cr absorbing layer from $t_a = 10\,\text{nm}$ to $t_a = 20\,\text{nm}$ (sample 8-9) increases the saturation of the resulting color, but at the cost of reduced transmission from 35 to 20% (Figure 4e). Nevertheless, semi-transparency is preserved. The order of the absorbing (Cr) and reflecting (Ag) layers have also been exchanged (Figure 4f), which reverses the order of the reflected colors to that observed in the structure with Cr layer on the substrate.

We have shown that the Janus effect can be seen in a semitransparent device with different colors reflected when the device is viewed from either the substrate side, i.e., from the direction of the absorbing layer, or the coating side, i.e., from the direction of the film with the higher reflectance. This leads to either a maximum or minimum in the reflectance spectrum creating either subtractive or additive color. The effect can be tuned by changing the thickness or dielectric constant of the dielectric cavity or a different choice of "absorber" or "reflector". Changing the thickness of the cavity shifts the hue of the reflected colors, while, the saturation of the colors can be

improved by increasing the thickness of the absorbing metal layer. Vivid colors are observed from both viewing directions in the sample with 10 nm of the silver film (reflective metal layer) and 20 nm of chromium film (absorbing metal layer) (Figure 4e).

Structural coloration using thin-film interference usually exhibits iridescence where the reflectance varies with the angle of observation.[31] The simulated optical response of the I-MIM device when illuminated at oblique incidence for *p*- and *s*-polarized illumination is shown in (**Figure 5**). The reflectance of the same device, when viewed at a near-normal angle of incidence (6°) was shown previously in Figure 2. The spectral features blue-shift with increasing angle of incidence leading to a change in the reflected color. For *p*-polarized light (a), a secondary minimum appears as the incident angle increases past 45°. These features correspond to the plasma wavelength of silver (390 nm (dotted lines)),[32] where there is a change in the optical properties. In the design considered, a more significant change of hue occurs for *s*-polarized illumination, as typically observed for thin-film MIM absorbers.[33]

A comparison between the simulated and measured reflection spectra for different angles of incidence and states of polarization for samples 1 – 4 is presented in **Figure 6**. The most striking iridescent effect occurs when samples are viewed from the coating side. This is more apparent for samples with "cool" colors at near-normal incidence such as cyan (sample 4) and magenta (samples 2 and 3). As the incident angle is increased, the hue changes from cooler shades to warmer colors (light pink for sample 4 and yellow for samples 2 and 3). The opposite effect seems to occur for incidence from the reverse substrate side, where samples with warmer colors at 6° (sample 4 (orange)) shift to cooler tones (green). The large tunability that these structures allow show potentials for applications in architecture, as decorative features, and as optical security features.

3. Conclusion

The research presented here shows that the optical Janus effect can be generated with a low number of uniform layers of

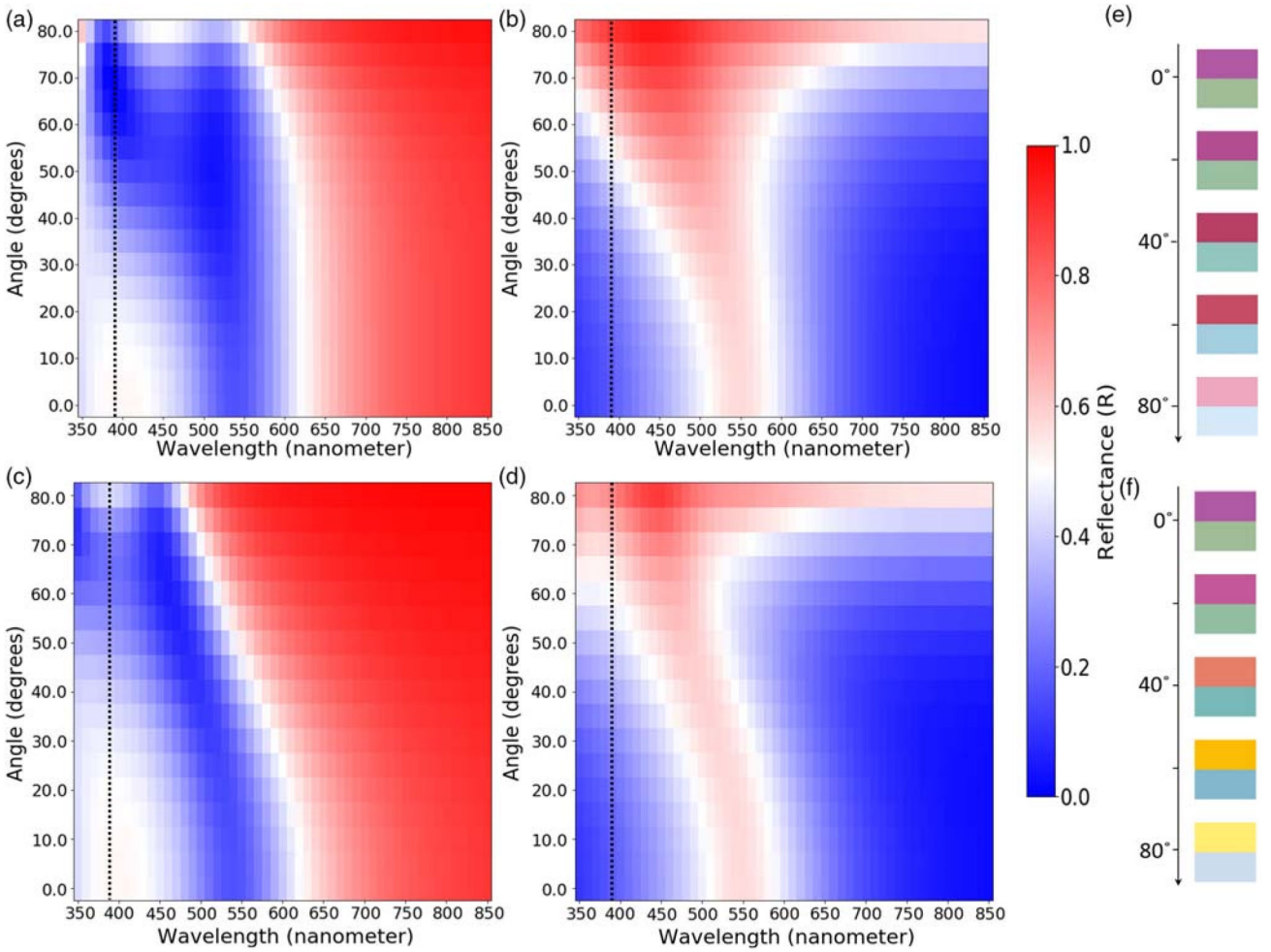

Figure 5. Reflectance (R) spectra of the I-MIM device at an increasing angle of incidence as viewed from: a,d) the coating and c,e) the substrate sides for: a,b) *p*-polarized and d,e) *s*-polarized light. Colors calculated from the spectra for: c) *p*-polarized and f) *s*-polarized light. The top half of the square demonstrates reflected color as viewed from the coating side, while the bottom half demonstrates color as viewed from the substrate side. The dotted lines indicate the plasma wavelength of Ag (390 nm).

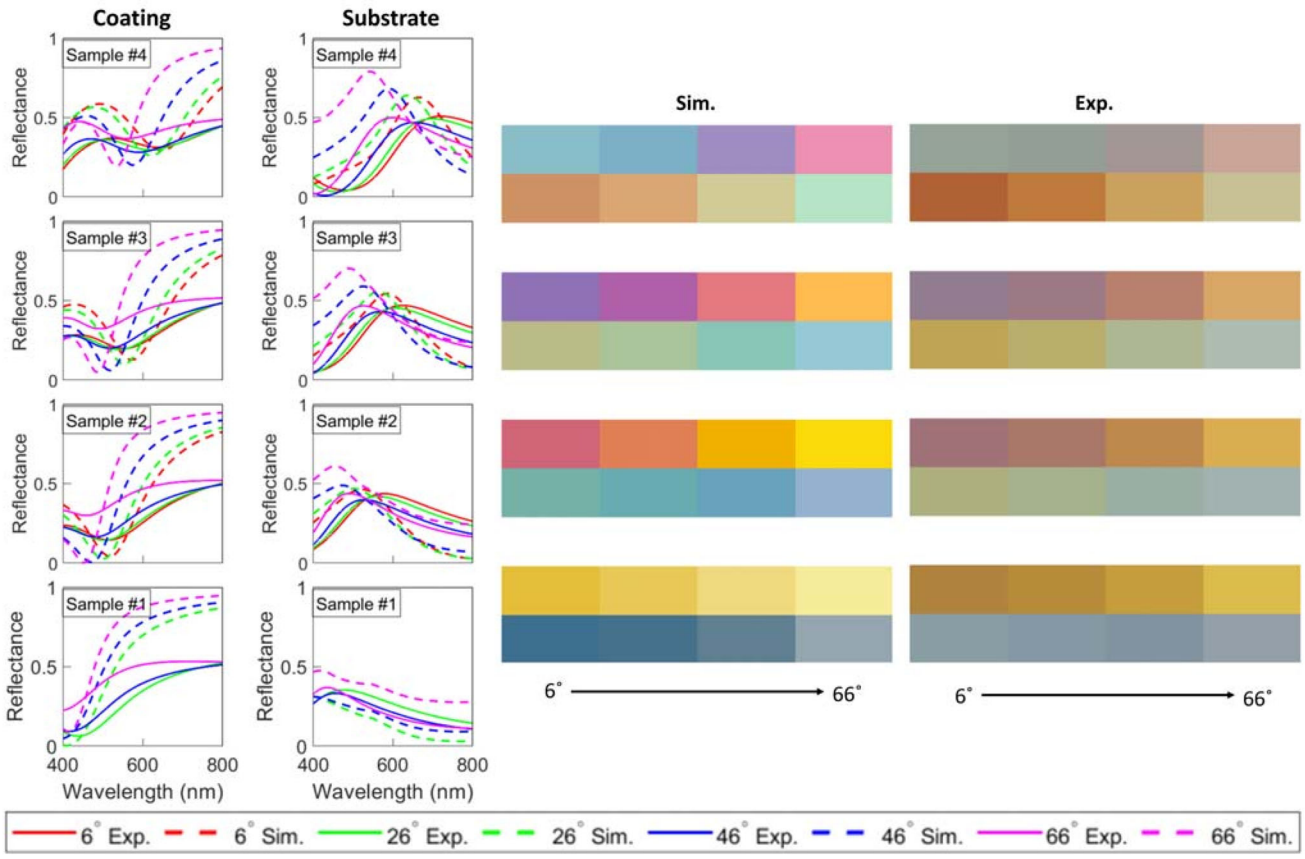

Figure 6. Measured (solid lines) and simulated (dashed lines) specular reflectance of samples 1 – 4 and the corresponding simulated (Sim.) and measured (Exp.) colors for *s*-polarized incident beam. The spectra exhibit blue shifts with increasing angles of incidence.

relatively inexpensive materials. The device exhibits different colors depending on the viewing direction through the asymmetric FP nanocavity structure formed by metal and insulator films. The role of geometry, specifically the cavity size and the thickness of the absorbing layer as well as the effect of materials were explored in the fabricated devices. The samples demonstrate an asymmetric color effect and the appearance of clear images in patterned areas, created by the selective removal of regions of one of the films, which are observable with the unaided eye. The device is semitransparent, with a transmission color that is independent of the viewing direction and is also iridescent. The simple fabrication processes required to generate a vibrant Janus color effect and to print macroscopic patterns mean the device has significant potential as a scalable optical security feature or to be used in applications in architecture or for the production of decorative features in consumer products. This is the first time the Janus effect has been demonstrated using continuous metal films with only SiO_2 as the dielectric material. Given the potential applications of the device, future developments could include replacing the rigid substrate with a flexible polymer or introducing a degree of tunability through the incorporation of layers of tunable materials such as liquid crystals[34] or phase change materials,[35] substituting the absorbing layer by electrically conductive films ,[19,36] or via mechanical deformation.[37]

4. Experimental Section

Sample Patterning: A mask was produced via direct-write photolithography (SF100 XPRESS, Intelligent Micro Patterning). After the exposure, unexposed photoresists on the wafers were dissolved in the developer solution. a chromium film was evaporated onto the sample at a rate of 0.5 Å /second via electron beam evaporation (Nanochrome II, Intlvac). The lift-off process was performed by soaking the sample in acetone, which dissolved the remaining photoresists and removed the metal layer that has been deposited on top of the resists.

Thin Films Deposition: The SiO_2 layer that forms the cavity spacing was deposited via PECVD (PLASMALAB100, Oxford Instruments) at a rate of 70 nm/minute. Then, the silver and the top SiO_2 layers were evaporated (Nanochrome II, Intlvac) consecutively at a rate of 0.5 Å /second.

Characterization: The colors of the devices under ambient illumination were captured using a camera (Nikon J1). Polarization- and angle-resolved reflectance and transmission measurements were performed using a commercial spectrophotometer (Cary 7000 Universal Measurement Spectrophotometer, Agilent). The measured reflectance was normalized to the incident power with respect to a calibration standard (STAN-SSH, Ocean Optics). In the case of transmission, the spectra were normalized to the measured power in the absence of the standard.

Simulation: Numerical simulations of the optical response of the proposed structure are performed using a custom MATLAB script and the resulting colors are computed using the transfer-matrix method.[24] Colors corresponding to the simulated and measured spectra are calculated by mapping the spectra to the 1931 CIE diagram, assuming standardized broadband daylight (D65).

Supporting Information

Supporting Information is available from the Wiley Online Library or from the author.

Acknowledgements

This research was funded by the Australian Government through the Australian Research Council. This work was performed in part at the Melbourne Centre for Nanofabrication (MCN) in the Victorian Node of the Australian National Fabrication Facility (ANFF).

Conflict of Interest

The authors declare no conflict of interest.

Data Availability Statement

The data that support the findings of this study are available from the corresponding author upon reasonable request.

Keywords

absorption, anti-counterfeiting, multilayers, structural colors, thin films

Received: December 9, 2021
Published online:

[1] J. Sun, B. Bhushan, J. Tong, *RSC Advances* **2013**, *3*, 14862.
[2] B. Yang, H. Cheng, S. Chen, J. Tian, *Mater. Chem. Front.* **2019**, *3*, 750.
[3] G. T. England, J. Aizenberg, *Rep. Prog. Phys.* **2017**, *81*, 016402.
[4] F. Meng, M. M. Umair, K. Iqbal, X. Jin, S. Zhang, B. Tang, *ACS Appl. Mater. Interfaces* **2019**, *11*, 13022.
[5] K. Yoon, S. Choi, J. Paek, D. Im, J. Roh, J. Kwon, H. Kim, *J. Opt. Soc. Korea* **2014**, *18*, 616.
[6] K. Watanabe, T. Hoshino, K. Kanda, Y. Haruyama, S. Matsui, *Jpn. J. Appl. Phys.* **2004**, *44*, L48.
[7] P. Liu, L. Bai, J. Yang, H. Gu, Q. Zhong, Z. Xie, Z. Gu, *Nanoscale Adv.* **2019**, *1*, 1672.
[8] P. Kurt, D. Banerjee, R. E. Cohen, M. F. Rubner, *J. Mater. Chem.* **2009**, *19*, 8920.
[9] R. J. Potton, *Rep. Prog. Phys.* **2004**, *67*, 717.
[10] OECD/EUIPO, *Trade In Counterfeit And Pirated Goods: Mapping The Economic Impact*, OECD Publishing, Paris **2016**.
[11] W. Hong, Z. Yuan, X. Chen, *Small* **2020**, *16*, 16.
[12] W. Li, Y. Shi, Z. Chen, S. Fan, *Nat. Commun.* **2018**, *9*, 1.
[13] A. Saito, *Sci. Technol. Adv. Mater.* **2011**, *12*, 064709.
[14] K. Saito, T. Tatsuma, *ACS Photonics* **2016**, *3*, 1782.
[15] C. Li, M. Zhao, X. Zhou, H. Li, Y. Wang, X. Hu, M. Li, L. Shi, Y. Song, *Adv. Opt. Mater.* **2018**, *6*, 1800651.
[16] G. T. England, C. Russell, E. Shirman, T. Kay, N. Vogel, J. Aizenberg, *Advanced Materials* **2017**, *29*, 1606876.
[17] S. Butun, K. Aydin, *ACS Photonics* **2015**, *2*, 1652.
[18] J. Bi, Y. Wu, L. Li, S. Zhang, S. Wu, *Nanoscale* **2020**, *12*, 3220.
[19] J. Chen, Z. Wang, C. Liu, Z. Chen, X. Tang, Q. Wu, S. Zhang, G. Song, S. Cong, Q. Chen, Z. Zhao, *Adv. Mater.* **2021**, *33*, 2007314.
[20] T. Kim, E.-S. Yu, Y.-G. Bae, J. Lee, I. S. Kim, S. Chung, S.-Y. Lee, Y.-S. Ryu, *Light Sci App* **2020**, *9*, 175.
[21] A. Kristensen, J. K. W. Yang, S. I. Bozhevolnyi, S. Link, P. Nordlander, N. J. Halas, N. A. Mortensen, *Nat. Rev. Mater.* **2017**, *2*, 1.
[22] C.-S. Park, V. R. Shrestha, S.-S. Lee, D.-Y. Choi, *Sci. Rep.* **2016**, *5*, 8467.
[23] X. Yang, Q. Zhao, B. Han, X. Zhao, *Kuei Suan Jen Hsueh Pao/J. Chin. Ceram. Soc.* **2008**, *36*, 954.
[24] H. A. Macleod, *Thin-film optical filters*, CRC Press, Taylor & Francis Group, Boca Raton, **2018**.
[25] J. Kim, H. Oh, M. Seo, M. Lee, *ACS Photonics* **2019**, *6*, 2342.
[26] I. H. Malitson, *J. Opt. Soc. Am.* **1965**, *55*, 1205.
[27] P. B. Johnson, R. W. Christy, *Phys. Rev. B* **1974**, *9*, 5056.
[28] J. Y. Jiang, S. Pillai, M. Green, *Sci. Rep.* **2016**, *6*, 30605.
[29] F. Cheng, P.-H. Su, J. Choi, S. Gwo, X. Li, C.-K. Shih, *ACS Nano* **2016**, *10*, 9852.
[30] T. N. Nunley, N. S. Fernando, N. Samarasingha, J. M. Moya, C. M. Nelson, A. A. Medina, S. Zollner, *J. Vac. Sci. Technol. B* **2016**, *34*, 061205.
[31] S. Kinoshita, S. Yoshioka, J. Miyazaki, *Rep. Prog.Phys.* **2008**, *71*, 7.
[32] L. Wesemann, E. Panchenko, K. Singh, E. Della Gaspera, D. E. Gómez, T. J. Davis, A. Roberts, *APL Photonics* **2019**, *4*, 100801.
[33] S. W. Verbruggen, M. Keulemans, J. A. Martens, S. Lenaerts, *J. Phys. Chem. C* **2013**, *117*, 19142.
[34] M. E. McConney, M. Rumi, N. P. Godman, U. N. Tohgha, T. J. Bunning, *Adv. Opt. Mater.* **2019**, *7*, 1900429.
[35] K. Wilson, C. Marocico, L. Bradley, *J. Phys. D: Appl. Phys.* **2018**, *51*, 255101.
[36] Y. Lyu, S. Mou, Z. Ni, Y. Bai, Y. Sun, Z. Cheng, *Opt. Express* **2017**, *25*, 2.
[37] X. Zhang, C. Liu, L. Zhang, L. Jia, M. Shi, L. Chen, Y. Di, Z. Gan, *Adv. Funct. Mater.* **2021**, *31*, 2010406.